A Library of Second-Order Models for Synchronous Machines

Olaoluwapo Ajala, *Student Member, IEEE,* Alejandro Domínguez-García, *Member, IEEE,* Peter Sauer, *Life Fellow, IEEE,* and Daniel Liberzon, *Fellow, IEEE*

***Abstract*—This paper presents a library of second-order models for synchronous machines that can be utilized in power system dynamic performance analysis and control design. The models have a similar structure to that of the so-called classical model in that they consist of two dynamic states, the power angle and the angular speed. However, unlike the classical model, they find applications beyond first swing stability analysis, i.e., they can be utilized for multi-swing transient stability analysis. The models are developed through a systematic reduction of a nineteenth-order model using singular perturbation techniques. They are validated by comparing their response with that of the high-order model from which they were derived, as well as that of other synchronous machine models existing in the literature, such as the so-called two-axis model and the so-called one-axis model.**

***Index Terms*—Synchronous machines, Reduced-order modeling, Singular perturbation analysis.**

I. Introduction

DYNAMIC models of synchronous machines find applications in power system analysis, control design tasks, and education, with each application requiring models that capture dynamical phenomena relevant to the intended use. This has led to a proliferation of synchronous machine models in the literature with varying degrees of complexity, computational cost, and dimension of the underlying state-space [1], [2], [3], [4]. One such model is the so-called classical model advocated in [5] and [6], a second-order dynamic model that captures the dynamics of the machine's phase and angular speed.

Analytically, the classical model is the simplest synchronous machine dynamical model, and this has made it a suitable candidate for modeling synchronous machine dynamics in a large class of system analysis and control design problems [7], [8], [9], [10], [11]. However, the classical model has a certain characteristic that restricts the class of problems it can be used for: it is only useful for first swing stability analysis, i.e., stability analysis for the first second after its equilibrium is perturbed [12], [13], [14]. As a result, if we consider that a power system may be stable in the first swing but unstable in subsequent swings, it is clear that the classical model, though simple, is unreliable for analysis and design tasks extending beyond a one-second time interval. For example, the design of a synchronization scheme for multiple generators, such as that presented in [15], requires synchronous machine models that capture the dynamics of each generator's phase, frequency, and voltage magnitude over the entire synchronization period. A second-order model such as the classical model should suffice, but the first swing stability constraint makes it unsuitable if the synchronization period exceeds one second. Although existing high-order models, such as the two-axis model and the one-axis model (see, e.g., [2], [16]), are clearly more accurate than the classical model, and therefore very useful for power system simulation, they are also significantly more detailed and computationally expensive. Consequently, they are, in general, analytically intractable for control design tasks requiring reduced-order models. There is therefore a need to develop models that possess the simplicity of the classical model, but also the accuracy and temporal breadth that such model lacks.

The main contribution of this paper is the development of three second-order synchronous machine models that have the same state-space dimension as the classical model, but are significantly more accurate (we will show that their accuracy is comparable to that of the two-axis model and the one-axis model). Using singular perturbation analysis as our main tool [2], [17], [18], [19], [20], the second-order models presented in this paper are derived by (i) identifying the fastest dynamic states in a nineteenth-order synchronous machine model; (ii) developing approximations of their manifolds, which are algebraic expressions; and (iii) replacing the differential equations for these states with the approximate algebraic expressions. The merit of these reduced-order models is that they all capture the effects of the excitation system and the speed governor on the synchronous machine's response. In addition to capturing these effects, the semi-damped model and the damped model also capture the effects of the damper windings on the synchronous machine's response.

Our approach to developing the proposed synchronous machine models is based on the developments in [2], [20], [21], where zero-order and/or first-order approximations of manifolds for fast dynamic states are used to develop ninth-order, eighth-order, fourth-order, and third-order models. However, this paper takes a step beyond these existing works by using the same approach to systematically develop second-order synchronous machine models. In addition, this paper is an extension of the work presented in [22], where approximations of manifolds for fast dynamic states are used to derive only one of the three models presented in this paper.

The remainder of this paper is organized as follows. In Section II, we present a high-order synchronous machine model that is adopted as the starting point for the development of our reduced-order models, and also briefly review the

The authors are with the Department of Electrical and Computer Engineering, University of Illinois at Urbana-Champaign, Urbana, IL 61801 USA. E-mail:{ooajala2, aledan, psauer, liberzon}@ILLINOIS.EDU.

classical model. In Section III, we present our main result, namely a library of second-order generator models, along with numerical simulations to validate their accuracy. In Section IV, a derivation of the proposed second-order models is presented in detail, and finally, in Section V, we comment on the implications of the presented results.

II. Preliminaries

In this section, we present the high-order model used as the starting point in this work. Afterwards, we introduce the so-called classical model and describe how it can be obtained from the aforementioned high-order model.

A. High-Order Synchronous Machine Model

The nineteenth-order synchronous machine model we describe in this section is based on the developments in [2], [3]. The setting includes a wound-rotor synchronous machine with three damper windings, an IEEE type DC1A excitation system [23], and a Woodward diesel governor (DEGOV1) [24] coupled to a diesel engine, which acts as the prime mover. Next, we provide mathematical expressions that describe the dynamic behavior of these components. The models presented hereafter are based on the following reasonable assumption.

Assumption 1. *The synchronous generator is connected to a bus in an electrical network through a short transmission line with series resistance, $R > 0$, and series reactance $X > 0$.*

Unless stated otherwise, each model is presented in a $qd0$ reference frame that is rotating at the speed of the synchronous machine. Also, all parameters and variables are scaled, and normalized using the per-unit system (see [2] for more details on the scaling and normalizing of each parameter, and see [3] for more details on $qd0$ transformation). First, we define the following parameters:

$$\begin{aligned} R_s &\coloneqq \tilde{R}_s + R, & X_k &\coloneqq \tilde{X}_k + X, \\ X_q &\coloneqq \tilde{X}_q + X, & X_d &\coloneqq \tilde{X}_d + X, \\ X_{q'} &\coloneqq \tilde{X}_{q'} + X, & X_{d'} &\coloneqq \tilde{X}_{d'} + X, \\ X_{q''} &\coloneqq \tilde{X}_{q''} + X, & X_{d''} &\coloneqq \tilde{X}_{d''} + X, \\ \tilde{X}_q &\coloneqq \tilde{X}_k + X_{mq}, & \tilde{X}_d &\coloneqq \tilde{X}_k + X_{md}, \end{aligned} \tag{1}$$

where $\tilde{R}_s$ denotes the per-phase stator resistance, $\tilde{X}_k$ denotes the synchronous machine's leakage reactance, X_{mq} and X_{md} denote the mutual reactances associated with the quadrature axis (q-axis) and direct axis (d-axis), respectively, $\tilde{X}_q$ and $\tilde{X}_d$ denotes stator winding reactances associated with the q-axis and d-axis, respectively, $\tilde{X}_{q'}$ and $\tilde{X}_{d'}$ denote transient reactances associated with the q-axis and d-axis, respectively, $\tilde{X}_{q''}$ and $\tilde{X}_{d''}$ denote sub-transient reactances associated with the q-axis and d-axis, respectively. [Note that for salient pole machines, $\tilde{X}_q = \tilde{X}_{q'}$, and for round-rotor machines, $\tilde{X}_q = \tilde{X}_d$]

1) Stator and rotor windings: Let $\tilde{\Psi}_q(t)$ and $\tilde{\Psi}_d(t)$ denote the q-axis and d-axis components of flux linkages for the stator windings, respectively, and let $E_{q'}(t)$ denote the flux linkage of the field/rotor winding. Also, let $\Phi_q(t)$and $\Phi_d(t)$ denote the q-axis and d-axis components of flux linkages for the electrical lines that the stator windings are connected to, respectively, and let $I_q(t)$ and $I_d(t)$ denote the q-axis and d-axis components of the stator output current, respectively. Let $\omega(t)$ denote the machine angular speed, in electrical radians per second, and let $\delta(t)$ denote the power angle of the synchronous machine in electrical radians. At the electrical network bus, let $V(t)$ and $\theta(t)$ denote the voltage magnitude and the voltage phase relative to a reference frame rotating at the nominal frequency, in electrical radians, respectively. Let $E(t)$ and $\tilde{\theta}(t)$ denote the synchronous machine's output voltage magnitude and voltage phase relative to a reference frame rotating at the nominal frequency, respectively. Then,

$$\dot{\delta} \coloneqq \omega - \omega_0, \tag{2}$$

the stator winding dynamics are described by:

$$\begin{aligned} \frac{1}{\omega_0}\dot{\Psi}_q &= -\frac{\omega}{\omega_0}\Psi_d + V_q + R_s I_q, \\ \frac{1}{\omega_0}\dot{\Psi}_d &= \frac{\omega}{\omega_0}\Psi_q + V_d + R_s I_d, \\ \frac{1}{\omega_0}\dot{\Phi}_q &= RI_q - \frac{\omega}{\omega_0}\Phi_d - E_q + V_q, \\ \frac{1}{\omega_0}\dot{\Phi}_d &= RI_d + \frac{\omega}{\omega_0}\Phi_q - E_d + V_d, \end{aligned} \tag{3}$$

and the field/rotor winding dynamics are described by:

$$\begin{aligned} \tau_{d'}\dot{E}_{q'} = &-(X_d - X_{d'})\left(I_d - \frac{X_{d'} - X_{d''}}{(X_{d'} - X_k)^2}(\Phi_{d_1}\right. \\ &\left. +(X_{d'} - X_k)I_d - E_{q'})\right) - E_{q'} + E_f, \end{aligned} \tag{4}$$

where $E_f(t)$ denotes the output voltage of the machine's excitation system (see Section II-A3 for a model describing its evolution), and

$$\begin{aligned} \Psi_q &= -X_{q''}I_q + \frac{X_{q'} - X_{q''}}{X_{q'} - X_k}\Phi_{q_2} - \frac{X_{q''} - X_k}{X_{q'} - X_k}E_{d'}, \\ \Psi_d &= -X_{d''}I_d + \frac{X_{d'} - X_{d''}}{X_{d'} - X_k}\Phi_{d_1} + \frac{X_{d''} - X_k}{X_{d'} - X_k}E_{q'}, \end{aligned} \tag{5}$$

where $\Phi_{q_2}(t)$ and $E_{d'}(t)$ denote the flux linkages of two damper windings aligned with the q-axis of the synchronous machine, and $\Phi_{d_1}(t)$ denotes the flux linkage of a damper winding aligned with the d-axis of the synchronous machine (see Section II-A2 for a model describing their evolution), and

$$\begin{aligned} \Phi_q &\coloneqq -XI_q, & \Phi_d &\coloneqq -XI_d, \\ \Psi_q &\coloneqq \tilde{\Psi}_q + \Phi_q, & \Psi_d &\coloneqq \tilde{\Psi}_d + \Phi_d, \\ V_q &\coloneqq V\cos(\delta - \theta), & V_d &\coloneqq V\sin(\delta - \theta), \\ E_q &\coloneqq E\cos(\delta - \tilde{\theta}), & E_d &\coloneqq E\sin(\delta - \tilde{\theta}), \\ \Psi &\coloneqq \Psi_q - \mathrm{j}\Psi_d, & \tilde{\Psi} &\coloneqq \tilde{\Psi}_q - \mathrm{j}\tilde{\Psi}_d. \end{aligned} \tag{6}$$

where ω_0 denotes the nominal frequency in electrical radians per second, and $\tau_{d'} = \frac{X_{kf} + X_{md}}{\omega_0 R_f}$, with X_{kf} denoting the leakage reactance of the field winding and R_f denoting the equivalent resistance of the field winding.

The output voltage and current of the high-order synchronous machine model is governed by the dynamics of the stator windings flux linkages, as well as those of the electrical lines that the stator windings are connected to. This relation is described by the dynamic circuit shown in Fig. 1 below.

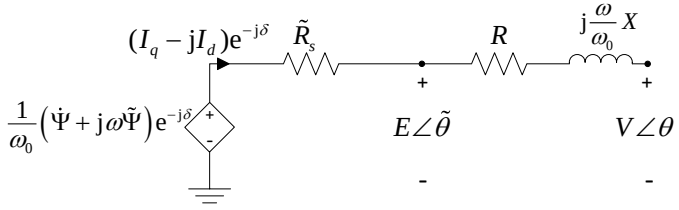

Fig. 1: The dynamic circuit associated with the high-order synchronous machine model.

2) Damper windings: The evolution of the flux linkages of the two damper windings aligned with the q-axis, $\Phi_{q2}(t)$ and $E_{d'}(t)$ respectively, and the single damper winding aligned with the d-axis, $\Phi_{d1}(t)$, is governed by:

$$\begin{aligned}\tau_{q''}\dot{\Phi}_{q_2} &= -\Phi_{q_2} - (X_{q'} - X_k)I_q - E_{d'},\\ \tau_{d''}\dot{\Phi}_{d_1} &= -\Phi_{d_1} - (X_{d'} - X_k)I_d + E_{q'},\end{aligned} \tag{7}$$

and

$$\begin{aligned}\tau_{q'}\dot{E}_{d'} = &-E_{d'} + (X_q - X_{q'})\left(I_q - \frac{X_{q'} - X_{q''}}{(X_{q'} - X_k)^2}\left(\Phi_{q_2}\right.\right.\\ &\left.\left.+(X_{q'} - X_k)I_q - E_{d'}\right)\right),\end{aligned} \tag{8}$$

where $\tau_{q''} = \frac{1}{\omega_0 R_{q_2}}\left(X_{kq_2} + X_{mq}\right)$, $\tau_{d''} = \frac{1}{\omega_0 R_{d_1}}\left(X_{k_1} + \frac{X_{md}X_{kf}}{X_{md}+X_{kf}}\right)$ and $\tau_{q'} = \frac{X_{kq_1}+X_{mq}}{\omega_0 R_{q_1}}$ are time constants, with X_{kq_2}, X_{kd_1}, and X_{kq_1} denoting the leakage reactances of its associated damper windings, and R_{q_2}, R_{d_1}, and R_{q_1} denoting their equivalent resistances.

3) Excitation system: We make the following assumption on the machine's magnetic saturation.

Assumption 2. *The effects of magnetic saturation on the machines excitation system are negligible.*

Then, the evolution of the output voltage of the machine's excitation system, $E_f(t)$, the exciter's control input, $U_f(t)$, and the rate feedback variable of the voltage regulation, $\bar{U}_f(t)$, is described by:

$$\begin{aligned}\tau_f\dot{E}_f &= -K_f E_f + U_f,\\ \tau_u\dot{U}_f &= -U_f + K_u\bar{U}_f - \frac{K_u\bar{K}_u}{\bar{\tau}_u}E_f + K_u(E_r - E),\\ \bar{\tau}_u\dot{\bar{U}}_f &= -\bar{U}_f + \frac{\bar{K}_u}{\bar{\tau}_u}E_f,\end{aligned} \tag{9}$$

where E_r denotes the voltage magnitude set-point of the synchronous machine, $\tau_f = \frac{L_f}{K_g}$, $K_f = \frac{\bar{R}_f}{K_g}$, $\bar{\tau}_u = \frac{L_t+L_m}{R_t}$, $\bar{K}_u = \frac{N_{t2}}{N_{t2}}\frac{L_m}{R_t}$, τ_u denotes the amplifier time constant, K_u denotes the amplifier gain, L_f denotes the unsaturated field inductance, K_g denotes the slope of the unsaturated portion of the exciter saturation curve, $\bar{R}_f$ denotes the resistance of the exciter circuit, L_t and L_m denote the series and magnetizing inductances of the stabilizing transformer that is used to stabilize the excitation system through voltage feedback [2], R_t denotes the series resistance of the stabilizing transformer, and $\frac{N_{t2}}{N_{t1}}$ denotes the turns ratio of the stabilizing transformer.

4) Speed governor and prime mover: Let $T_m(t)$ denote the mechanical torque output of the machine. For the speed governor system, let $P_{a_2}(t)$ denote the output of its actuator and let $P_{b_2}(t)$ denote the output of its electric control box. Let $P_u(t)$ denote the valve position of the diesel engine, which acts as the prime mover. Then, the angular speed of the synchronous machine is described by the expression:

$$M\dot{\omega} = T_m - \Psi_d I_q + \Psi_q I_d - \tilde{D}_0\omega, \tag{10}$$

and the speed control system of the synchronous machine can be described by:

$$\begin{aligned}\tau_m\dot{T}_m &= -T_m + P_u, & \dot{P}_u &= P_{a_1} + \tau_4 P_{a_2},\\ \dot{P}_{a_1} &= P_{a_2}, & \dot{P}_{b_1} &= P_{b_2},\\ \tau_{a_2}\dot{P}_{a_2} &= -\frac{1}{\tau_5+\tau_6}\left(P_{a_1} - \kappa\left(P_{b_1} + \tau_3 P_{b_2}\right)\right) - P_{a_2},\\ \tau_2\dot{P}_{b_2} &= \frac{1}{\tau_1}\left(\frac{1}{\bar{D}_0\omega_0}\left(P_c - P_u\right) - \frac{1}{\omega_0}(\omega - \omega_0)\right)\\ &\quad - P_{b_2} - \frac{1}{\tau_1}P_{b_1},\end{aligned} \tag{11}$$

where τ_1, τ_2, τ_3 , τ_4, τ_5 and τ_6 denote time constants of the control system, $\tau_{a_2} = \frac{\tau_5\tau_6}{\tau_5+\tau_6}$, κ denotes a controller gain for the actuator, P_c denotes the active power set-point of the machine, M denotes the inertia of the machine, $\tilde{D}_0$ denotes the friction and windage damping coefficient of the machine, τ_m denotes the time constant of the engine, and $\bar{D}_0 = \frac{1}{R_D\omega_0}$, where R_D denotes the droop coefficient of the machine.

B. Classical Model

The classical model of a synchronous machine is a second-order model whose formulation is based on the following assumptions [25]: (i) the machine can be modeled as a constant magnitude voltage source with a series reactance, (ii) the mechanical rotor angle of the machine can be represented by the angle of the voltage source plus a constant, (iii) the effects of damper windings can be neglected, and (iv) the machine mechanical power input is constant. Thus, the classical model can be obtained from the high-order model by setting $\tau_{q''} = 0$, $\tau_{d''} = 0$, $\frac{1}{\omega_0} = 0$, $\frac{\omega(t)}{\omega_0} = 1$, $\tilde{R}_s = 0$, $R_e = 0$, $\tilde{X}_{q'} = \tilde{X}_{d'}$, $\tau_{q'} = \infty$, $\tau_{d'} = \infty$, and $\tau_m = \infty$, yielding:

$$\begin{aligned}\dot{\delta} &= \omega - \omega_0,\\ M\dot{\omega} &= T_m(0) - \tilde{D}_0\omega - \frac{\tilde{E}V}{X_{d'}}\sin(\delta + \tilde{\delta} - \theta),\end{aligned} \tag{12}$$

where $\tilde{E}$ and $\tilde{\delta}$ are constants taking values:

$$\tilde{E} = \sqrt{\left(E_{q'}(0)\right)^2 + \left(E_{d'}(0)\right)^2}, \quad \tilde{\delta} = \arctan\left(\frac{-E_{d'}(0)}{E_{q'}(0)}\right).$$

III. A Library of Second-Order Models

In this section, we first provide a brief summary of our main result, namely three second-order synchronous machine models referred to as (i) the elemental model, (ii) the semi-damped model, and (iii) the damped model; their detailed

TABLE I: Expressions for $\tilde{E}_q(\cdot)$, $\tilde{E}_d(\cdot)$, $\tilde{X}$, and $T_m(t)$ (see Sections II and IV for details).

	Expression for $\tilde{E}_q(\cdot)$	Expression for $\tilde{E}_d(\cdot)$	Expression for $\tilde{X}$	Expression for $T_m(t)$
Classical model	$E_{q'}(0)$	$E_{d'}(0)$	$\tilde{X}_{d'}$	$T_m(0)$
Elemental model	$\frac{K_u}{K_f}(E_r - E(t))$	$(X_d - X_q)I_q(t)$	$\tilde{X}_d$	$P_c - \bar{D}_0(\omega(t) - \omega_0)$
Semi-damped model	$\frac{K_u}{K_f}(E_r - E(t))$	$(X_d - X_q)I_q(t) + \frac{\tau_{q'}(X_q - X_{q'})}{X_q}\frac{\mathrm{d}\,(V(t)\sin(\delta(t)-\theta(t)))}{\mathrm{d}t}$	$\tilde{X}_d$	$P_c - \bar{D}_0(\omega(t) - \omega_0)$
Damped model	$\frac{K_u}{K_f}(E_r - E(t)) - K_d X_d \frac{\mathrm{d}\,(V(t)\cos(\delta(t)-\theta(t)))}{\mathrm{d}t}$	$(X_d - X_q)I_q(t) + K_q X_q \frac{\mathrm{d}\,(V(t)\sin(\delta(t)-\theta(t)))}{\mathrm{d}t}$	$\tilde{X}_d$	$P_c - \bar{D}_0(\omega(t) - \omega_0)$

derivation is provided in Section IV. Afterwards, we provide numerical simulations comparing the performance of the proposed models with that of the high-order model from which they were derived, and that of other previously proposed reduced-order models, namely the classical model, the two-axis model, and the one-axis model.

A. The Second-Order Synchronous Machine Models

Figure 2 depicts a circuit describing the relation between the output voltage and current of our proposed second-order synchronous machine models, and a phasor diagram that describes the relationship between the circuit parameters. The evolution of the controlled voltage source angle, $\delta(t)$, is governed by

$$\begin{aligned} \dot{\delta} &= \omega - \omega_0, \\ M\dot{\omega} &= \overbrace{\underbrace{P_c}_{\substack{\text{active power}\\ \text{set-point}}} \underbrace{- \bar{D}_0(\omega - \omega_0)}_{\substack{\text{speed governor}\\ \text{torque}}}}^{T_m} - \underbrace{\tilde{D}_0\omega}_{\substack{\text{friction \& windage}\\ \text{damping torque}}} \\ &\quad \underbrace{- \frac{\tilde{E}(\cdot)V}{\tilde{X} + X}\sin(\delta + \tilde{\delta}(\cdot) - \theta)}_{\text{torque of electrical origin}}, \end{aligned} \tag{13}$$

where

$$\tilde{E}(\cdot) \coloneqq \sqrt{\tilde{E}_q(\cdot)^2 + \tilde{E}_d(\cdot)^2}, \quad \tilde{\delta}(\cdot) \coloneqq \arctan\left(\frac{-\tilde{E}_d(\cdot)}{\tilde{E}_q(\cdot)}\right),$$

with the specific expressions for $\tilde{E}_q(\cdot)$ and $\tilde{E}_d(\cdot)$ given in Table I.

The three proposed models capture the effects of the excitation system and the speed governor on the synchronous machine's response. However, both the semi-damped model and the damped model approximate the effects of the damper windings through the use of a first-order algebraic expression—the elemental model uses a zero-order algebraic expression for this approximation. The semi-damped model performs this first-order approximation for only one damper winding, whereas the damped model performs it for all the damper windings. The semi-damped model is only applicable for round-rotor machines because the damper windings whose effects it approximates with a first-order expression are typically only used in round-rotor machines (see [3], pp. 276–278, for more details).

In comparison with the classical model, the proposed models also represent a controlled voltage source behind a series reactance. However, unlike the classical model, the series reactance of our proposed models has a value equal to $\tilde{X}_d$, not $\tilde{X}_{d'}$, and the mechanical torque, $T_m(t)$, is time-varying, not constant. Also, the controlled voltage source has a value that is not a constant, but is a function of multiple states.

B. Numerical Validation

Using two test scenarios, we compare the performance of our proposed models to that of the high-order model from which they were derived, the two-axis model, the one-axis model, and the classical model. The generator high-order model parameters and the transmission line parameters are collected in Table II.

The two-axis model is a two-winding model that is derived from the high-order model by replacing the differential equations in (3) and (7) with a zero-order integral manifold, whereas the one-axis model is a one-winding model that is derived by from the two-axis model by replacing the differential equation in (8) with a zero-order integral manifold [2], [16]. The two-axis model is referred to as a two-winding model because it comprises two differential equations that describe the dynamics of two windings, the field/rotor winding and one of two damper windings aligned with the q-axis. The one-axis model is referred to as a one-winding model

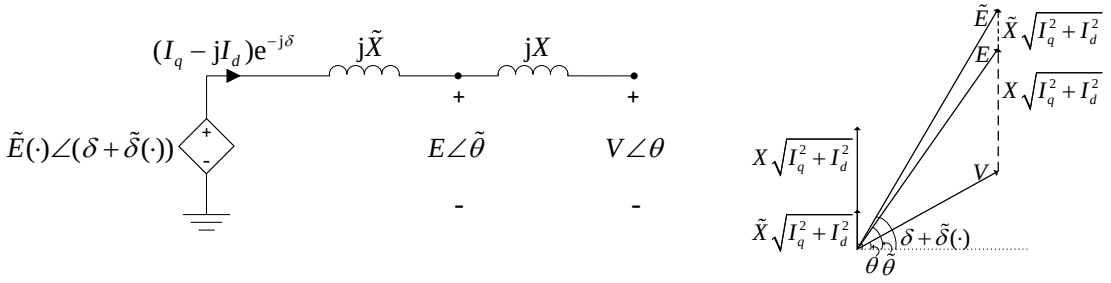

(a) Dynamic circuit. (b) Phasor diagram.

Fig. 2: The dynamic circuit and phasor diagram associated with the second-order synchronous machine models.

because it comprises one differential equation that describes the dynamics of the field/rotor winding.

TABLE II: System parameters for a round-rotor synchronous machine connected to a transmission line

	parameter	value
Damper windings	$\tau_{q''}$	0.9453 [s]
	$\tau_{d''}$	0.042 [s]
	$\tau_{q'}$	3.6123 [s]
	$\tilde{X}_{q''}$	0.2388 [pu]
	$\tilde{X}_{q'}$	0.7299 [pu]
	$\tilde{X}_q$	1.7997 [pu]
	$\tilde{X}_k$	0.19 [pu]
Stator windings	ω_0	376.99 [rad/s]
	R_s	0.003 [pu]
	$\tilde{X}_{d''}$	0.24 [pu]
	$\tilde{X}_{d'}$	0.32 [pu]
IEEE DC1A exciter	$\tau_{d'}$	5.0141 [s]
	τ_f	1×10^{-8} [s]
	τ_u	0.002 [s]
	$\bar{\tau}_u$	1×10^{-12} [s]
	$\tilde{X}_d$	1.7997 [pu]
	K_f	1 [pu]
	K_u	200
	$\bar{K}_u$	0 [s]
DEGOV1 speed governor	τ_1	1×10^{-4} [s]
	τ_2	0 [s]
	τ_3	0.5001 [s]
	τ_4	25×10^{-3} [s]
	τ_5	9×10^{-4} [s]
	τ_6	5.74×10^{-3} [s]
	τ_m	24×10^{-3} [s]
	κ	10
	P_c	0.05013 [pu]
	M	0.1188 [s^2]
	$\tilde{D}_0$	2.5825×10^{-7} [s/rad]
	$\bar{D}_0$	0.0531 [s/rad]
Transmission line	R	0.004 [pu]
	X	0.0595 [pu]

In the first test scenario, we consider the two-bus power system depicted in Fig. 3 comprising a synchronous machine connected to a constant power load through a transmission line. Let P and Q denote the active power output and reactive power output of the synchronous generator, in per-unit, respectively. The load's active power demand is increased from 0.05 pu to 0.25 pu at time $t = 30$ s, from 0.25 pu to 0.35 pu at time $t = 1530$ s, from 0.35 pu to 0.3 pu at time $t = 3030$ s, and from 0.3 pu to 0.15 pu at time $t = 4530$ s. For each load change, the reference voltage magnitude E_r is changed to keep the bus voltage magnitude at $V = 1$ pu. The phase response, angular frequency response, voltage magnitude response, and output power response of each synchronous machine model to this test scenario is depicted in Figs. 5 – 9, and the root mean square errors associated with these variables, relative to the high-order model, are recorded in Table III. The RMSE results show that the accuracy of the classical model is significantly poorer than that of the other models. The results also show that, for each variable considered, the root mean square errors associated with the two-axis model, the one-axis model, the damped model, the semi-damped model, and the elemental model have the same order of magnitude.

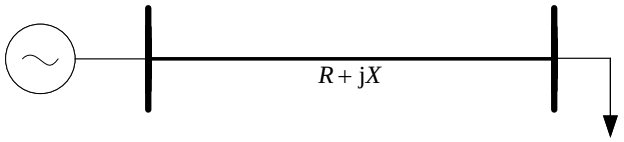

Fig. 3: A one-line diagram of the system in the first test scenario.

TABLE III: Root Mean Square Error (RMSE) for First Test Scenario

	δ (deg)	ω (rpm)	V (pu)	P (pu)	Q (pu)
two-axis model	1.00×10^3	2.74	4.52×10^{-3}	1.86×10^{-4}	2.66×10^{-3}
one-axis model	1.00×10^3	2.74	4.54×10^{-3}	1.86×10^{-4}	2.66×10^{-3}
damped model	1.07×10^3	2.92	3.49×10^{-3}	3.67×10^{-4}	3.91×10^{-3}
semi-damped model	1.07×10^3	2.92	3.49×10^{-3}	3.67×10^{-4}	3.91×10^{-3}
elemental model	1.07×10^3	2.92	3.49×10^{-3}	3.67×10^{-4}	3.91×10^{-3}
classical model	1.59×10^7	6.49×10^4	4.72×10^{-2}	3.67×10^{-4}	7.21×10^{-2}

In the second test scenario, we consider the two-bus power system depicted in Fig. 4 comprising a synchronous machine connected to a constant power load through two parallel transmission lines. At time $t = 60$ s, one of the transmission lines is disconnected from the load's bus. Let P and Q denote the active power output and reactive power output of the synchronous generator, in per-unit, respectively. The phase response, angular frequency response, voltage magnitude response, and output power response of each synchronous machine model to this test scenario is depicted in Figs. 10 – 14, and the root mean square errors associated with these variables, relative to the high-order model, are depicted in Table IV. The results also show that, for each variable considered, the root mean square errors associated with the damped model, the semi-damped model, the elemental model, and the classical model have the same order of magnitude. This is due to the fact that the resistance of the transmission lines are neglected in those models.

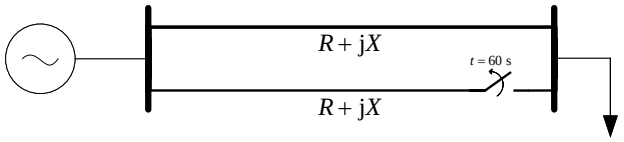

Fig. 4: A one-line diagram of the system in the second test scenario.

TABLE IV: Root Mean Square Error (RMSE) for Second Test Scenario

	δ (deg)	ω (rpm)	V (pu)	P (pu)	Q (pu)
two-axis model	1.57×10^{-5}	5.65×10^{-6}	9.79×10^{-6}	1.85×10^{-7}	3.35×10^{-7}
one-axis model	1.57×10^{-5}	5.65×10^{-6}	9.78×10^{-6}	1.85×10^{-7}	3.35×10^{-7}
damped model	4.00×10^{-3}	1.11×10^{-3}	4.57×10^{-5}	7.19×10^{-6}	5.25×10^{-6}
semi-damped model	4.00×10^{-3}	1.11×10^{-3}	4.58×10^{-5}	7.19×10^{-6}	5.25×10^{-6}
elemental model	4.00×10^{-3}	1.11×10^{-3}	4.58×10^{-5}	7.19×10^{-6}	5.25×10^{-6}
classical model	4.00×10^{-3}	1.11×10^{-3}	7.50×10^{-3}	7.18×10^{-6}	6.47×10^{-6}

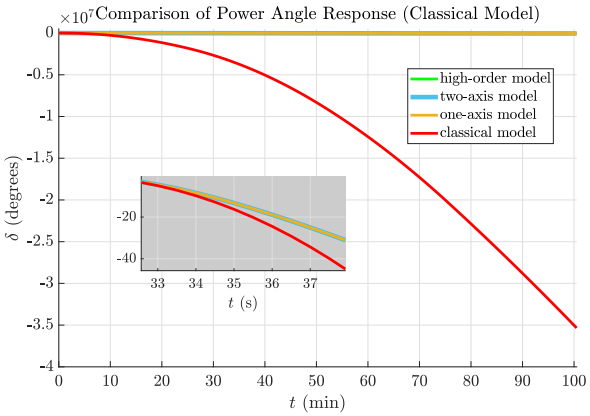

(a) The classical model.

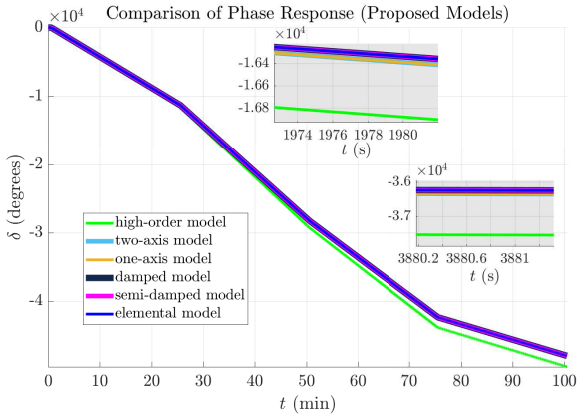

(b) The proposed models.

Fig. 5: First Test Scenario: Phase response of the classical model and the proposed models in comparison with those of the two-axis model, the one-axis model, and the high-order model.

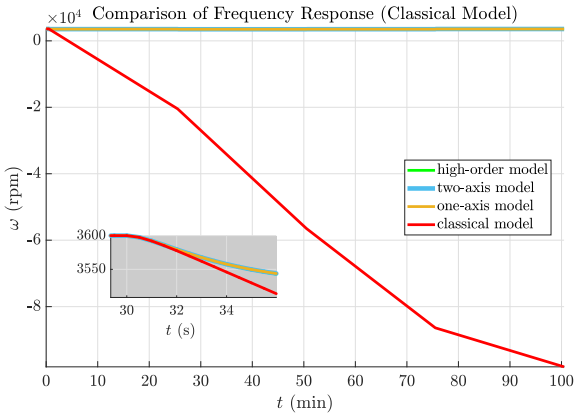

(a) The classical model.

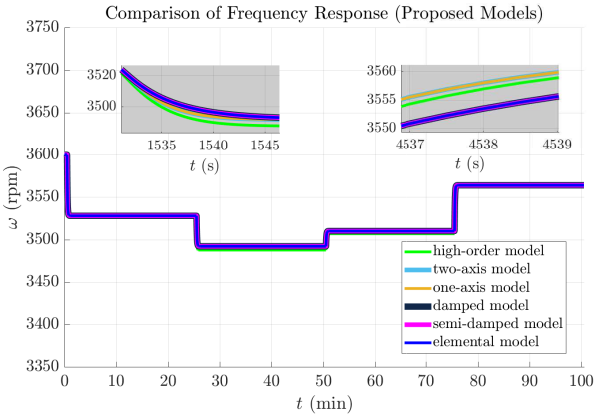

(b) The proposed models.

Fig. 6: First Test Scenario: Angular frequency response of the classical model and the proposed models in comparison with those of the two-axis model, the one-axis model, and the high-order model.

IV. Derivation of Proposed Second-Order Synchronous Machine Models

In this section, the elemental model, the semi-damped model, and the damped model, are derived from the nineteenth-order synchronous machine model presented in Section II-A, using singular perturbation analysis. We begin the section by presenting the time-scale properties of the high-order model. Afterwards, we derive the approximate manifolds that were utilized for the model-order reduction, and finally we present a derivation of the proposed second-order models.

A. Time-Scale Properties of the High-Order Model

The following observations are based on standard parameter values obtained from synchronous machine models in [1], [2], [3], [24], and an eigenvalue analysis of these models.

Observation 1. *The dynamics of* $\Psi_q(t)$, $\Psi_d(t)$, $E_{q'}(t)$, $\Phi_q(t)$, $\Phi_d(t)$, $\Phi_{q_2}(t)$, $\Phi_{d_1}(t)$, $E_{d'}(t)$, $E_f(t)$, $U_f(t)$, $\bar{U}_f(t)$, $T_m(t)$, $P_u(t)$, $P_{a_1}(t)$, $P_{a_2}(t)$, $P_{b_1}(t)$, *and* $P_{b_2}(t)$ *are much faster than those of* $\delta(t)$ *and* $\omega(t)$.

Observation 2. *For* $\epsilon = 0.1$ *denoting a constant, the parameters* R_s, $\tau_{q''}$, $\tau_{q'}$, $\frac{1}{\omega_0}$, τ_f, τ_u, $\bar{\tau}_u$, τ_m, τ_{a_2}, τ_2, τ_1, $(\tau_5+\tau_6)$, $\frac{\tau_5\tau_6}{(\tau_5+\tau_6)}$, $\frac{1}{\kappa R_D}$ *are* $\boldsymbol{\mathcal{O}}(\epsilon)$[1].

Based on these observations, the nineteenth-order model described by (2) – (11) can be expressed compactly as:

$$\dot{\boldsymbol{x}}(t) = f\left(\boldsymbol{x}(t), \boldsymbol{z}(t), \epsilon\right), \qquad \boldsymbol{x}(0) = \boldsymbol{x}^0, \tag{14}$$

$$\epsilon\dot{\boldsymbol{z}}(t) = g\left(\boldsymbol{x}(t), \boldsymbol{z}(t), \epsilon\right), \qquad \boldsymbol{z}(0) = \boldsymbol{z}^0, \tag{15}$$

where $\boldsymbol{x}(t) = \begin{bmatrix}\delta & \omega\end{bmatrix}^\top$, $\boldsymbol{z}(t) = \begin{bmatrix}\Psi_q & \Psi_d & \Phi_q & \Phi_d & \Phi_{q_2} & \Phi_{d_1} & E_{d'} & E_{q'} & E_f & U_f & \bar{U}_f & T_m & P_u & P_{a_1} & P_{a_2} & P_{b_1} & P_{b_2}\end{bmatrix}^\top$. In the remainder of this section, we refer to the elements of $\boldsymbol{z}(t)$ as the fast states, and elements of $\boldsymbol{x}(t)$ as the slow states. Other observations, which will prove useful in the model-order reduction process are:

Observation 3. *The dynamics of* Ψ_q, Ψ_d, Φ_q *and* Φ_d *are much faster than those of* Φ_{q_2}, Φ_{d_1},.

[1]Consider a positive constant $\epsilon < 1$, and a function $f(\epsilon)$, defined on some subset of the real numbers. We write $f(\epsilon) = \boldsymbol{\mathcal{O}}(\epsilon^i)$ if and only if there exists a positive real number k, such that: $\left|f(\epsilon)\right| \leq k\epsilon^i$, as $\epsilon \to 0$.

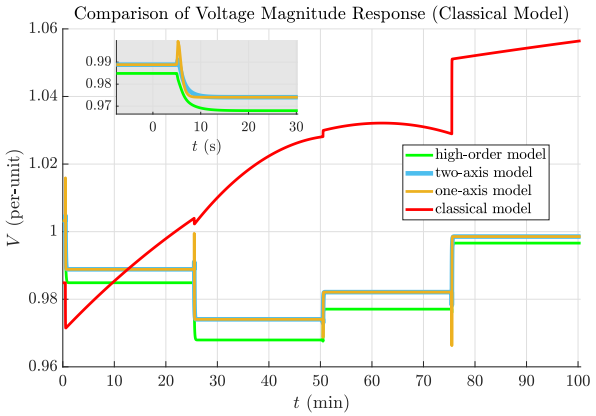

(a) The classical models.

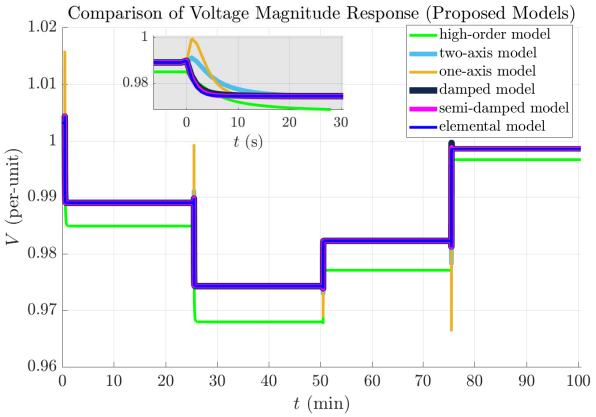

(b) The proposed model.

Fig. 7: First Test Scenario: Voltage magnitude response of the classical model and the proposed models in comparison with those of the two-axis model, the one-axis model, and the high-order model.

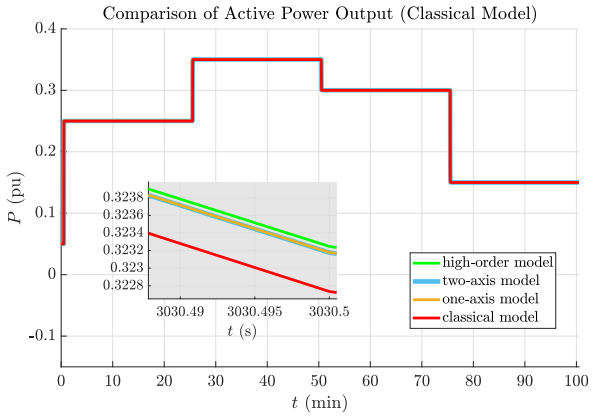

(a) The classical models.

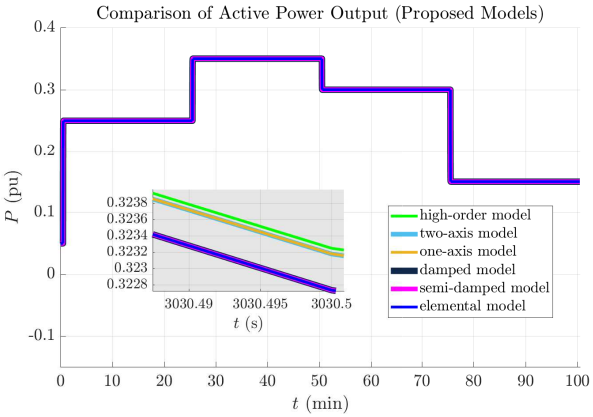

(b) The proposed model.

Fig. 8: First Test Scenario: Active power output response of the classical model and the proposed models in comparison with those of the two-axis model, the one-axis model, and the high-order model.

Observation 4. *The dynamics of Φ_{q_2} and Φ_{d_1} are much faster than those of $E_{q'}$, and $E_{d'}$.*

B. Manifold Approximations for Fast States

Employing singular perturbation analysis as described in [17], (14) and (15) can be reduced by replacing the differential equation (15) with a manifold approximation, which is an algebraic expression. Let '(0)', '(1)', and '(2)' superscripts be used to denote zero-order, first-order, and second-order terms, respectively. A manifold for $\boldsymbol{z}(t)$ can be expressed as a power series in ϵ to give:

$$\boldsymbol{z}(t) = \boldsymbol{z}^{(0)}(t) + \epsilon \boldsymbol{z}^{(1)}(t) + \epsilon^2 \boldsymbol{z}^{(2)}(t) + \cdots, \tag{16}$$

where $\boldsymbol{z}^{(0)}(t)$, $\boldsymbol{z}^{(1)}(t)$, and $\boldsymbol{z}^{(2)}(t)$ are algebraic functions whose arguments are elements of $\boldsymbol{x}(t)$. For small values of ϵ, the manifold's zero-order approximation is

$$\boldsymbol{z}(t) \approx \boldsymbol{z}^{(0)}(t), \tag{17}$$

and its first-order approximation is given by:

$$\boldsymbol{z}(t) \approx \boldsymbol{z}^{(0)}(t) + \epsilon \boldsymbol{z}^{(1)}(t). \tag{18}$$

To derive the expressions for $\boldsymbol{z}^{(0)}(t)$ and $\boldsymbol{z}^{(1)}(t)$, substitute (16) into (15) to give

$$\epsilon \frac{\mathrm{d}}{\mathrm{d}t}(\boldsymbol{z}^{(0)}(t) + \epsilon \boldsymbol{z}^{(1)}(t) + \epsilon^2 \boldsymbol{z}^{(2)}(t) + \cdots) \tag{19}$$

$$= g(\boldsymbol{x}(t), \boldsymbol{z}^{(0)}(t) + \epsilon \boldsymbol{z}^{(1)}(t) + \epsilon^2 \boldsymbol{z}^{(2)}(t) + \cdots, \epsilon). \tag{20}$$

The n-th order term, $\boldsymbol{z}^{(n)}(t)$, $n \in \{0, 1, 2, \dots\}$, is derived by equating the left-hand side and right-hand side terms that have like powers of ϵ^n, and solving for $\boldsymbol{z}^{(n)}(t)$ (see [17], for more details). Note that solving for $\boldsymbol{z}^{(0)}(t)$ in this manner is equivalent to setting $\boldsymbol{z}(t) = \boldsymbol{z}^{(0)}(t)$, $\epsilon = 0$ in (15) and solving for $\boldsymbol{z}^{(0)}(t)$.

C. Manifold Approximations for Fast States in the High-Order Synchronous Machine Model

We begin the model-order reduction process with the following assumptions on the angular speed of the synchronous machine and the per-phase line resistance.

Assumption 3. *The angular speed of the machine, $\omega(t)$, is sufficiently close to the nominal speed of the machine so that $\frac{\omega(t)}{\omega_0} = 1 + \boldsymbol{\mathcal{O}}(\epsilon)$.*

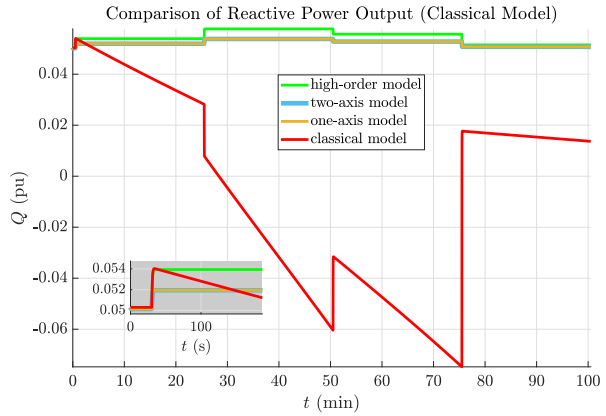

(a) The classical models.

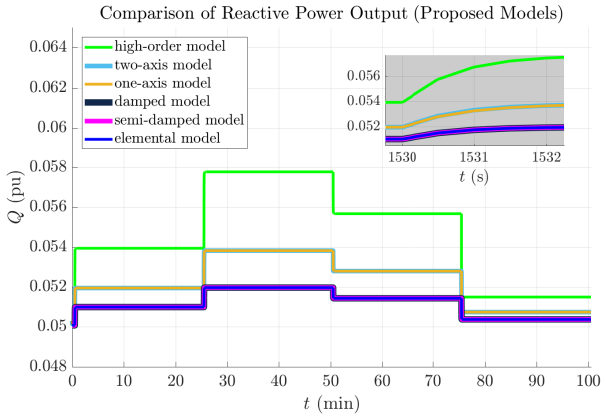

(b) The proposed model.

Fig. 9: First Test Scenario: Reactive power output response of the classical model and the proposed models in comparison with those of the two-axis model, the one-axis model, and the high-order model.

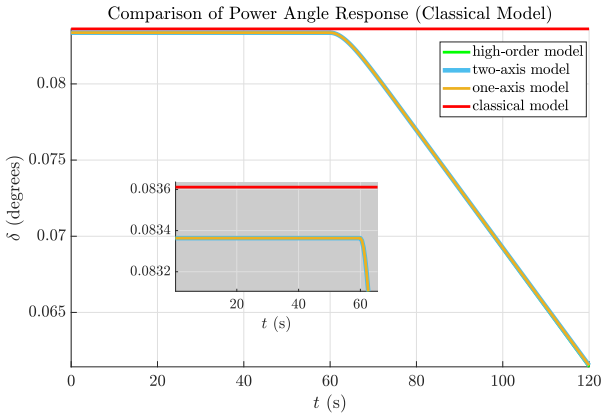

(a) The classical model.

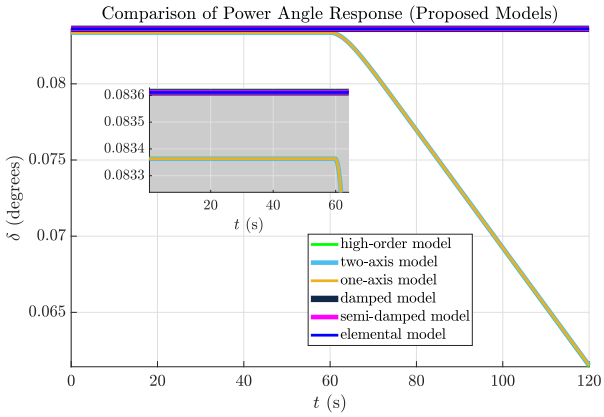

(b) The proposed models.

Fig. 10: Second Test Scenario: Phase response of the classical model and the proposed models in comparison with those of the two-axis model, the one-axis model, and the high-order model.

Assumption 4. *The per-phase line resistance, R is $\boldsymbol{\mathcal{O}}(\epsilon)$.*

Firstly, for the fastest dynamic states, i.e., $\Psi_q(t)$, $\Psi_d(t)$, $\Phi_q(t)$ and $\Phi_d(t)$, the following zero-order approximations of its manifolds are derived by setting $R_s = 0$, $\frac{\omega(t)}{\omega_0} = 1$, and employing singular perturbation analysis, as described in Section IV-B, on the system of equations in (3):

$$\begin{aligned}
\Psi_q &\approx \Psi_q^{(0)}(t) = -V_d,\\
\Psi_d &\approx \Psi_d^{(0)}(t) = V_q,\\
\Phi_q &\approx \Phi_q^{(0)}(t) = E_d - V_d,\\
\Phi_d &\approx \Phi_d^{(0)}(t) = -E_q + V_q.
\end{aligned} \tag{21}$$

For the second fastest states, i.e., $\Phi_{q_2}(t)$ and $\Phi_{d_1}(t)$, which are damper winding states, we derive the following first-order approximations of their manifolds by employing singular perturbation analysis, as described in Section IV-B, on the system of equations in (7):

$$\begin{aligned}
\Phi_{q_2} &\approx \Phi_{q_2}^{(0)}(t) + \tau_{q''}\Phi_{q_2}^{(1)}(t),\\
\Phi_{d_1} &\approx \Phi_{d_1}^{(0)}(t) + \tau_{d''}\Phi_{d_1}^{(1)}(t),
\end{aligned} \tag{22}$$

where

$$\begin{aligned}
\Phi_{q_2}^{(0)}(t) =& -\frac{X_k}{X_{q'}}E_{d'} - \frac{X_{q'} - X_k}{X_{q'}}V_d,\\
\Phi_{q_2}^{(1)}(t) =& -\frac{X_{q''}X_kX_q}{\tau_{q'}(X_{q'})^3}E_{d'} + \frac{X_{q''}X_k(X_q - X_{q'})}{\tau_{q'}(X_{q'})^3}V_d\\
&+ \frac{X_{q''}(X_{q'} - X_k)}{(X_{q'})^2}\dot{V}_d,\\
\Phi_{d_1}^{(0)}(t) =& \frac{X_k}{X_{d'}}E_{q'} + \frac{X_{d'} - X_k}{X_{d'}}V_q,\\
\Phi_{d_1}^{(1)}(t) =& \frac{X_{d''}X_kX_d}{\tau_{d'}(X_{d'})^3}E_{q'} - \frac{X_{d''}X_k(X_d - X_{d'})}{\tau_{d'}(X_{d'})^3}V_q\\
&- \frac{X_{d''}(X_{d'} - X_k)}{(X_{d'})^2}\dot{V}_q - \frac{X_{d''}X_k}{\tau_{d'}(X_{d'})^2}E_f.
\end{aligned}$$

For the subsequent fastest state, i.e., $E_{d'}(t)$, which is the slowest damper winding state, we derive the following first-order approximation of its manifold by employing singular perturbation analysis, as described in Section IV-B, on (8):

$$E_{d'} \approx E_{d'}^{(0)}(t) + \tau_{q'}E_{d'}^{(1)}(t),$$

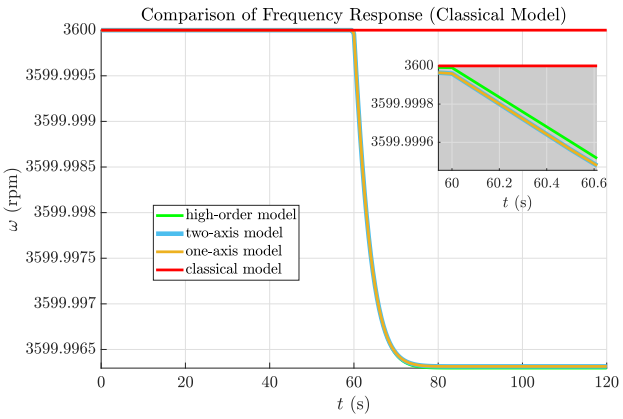

(a) The classical model.

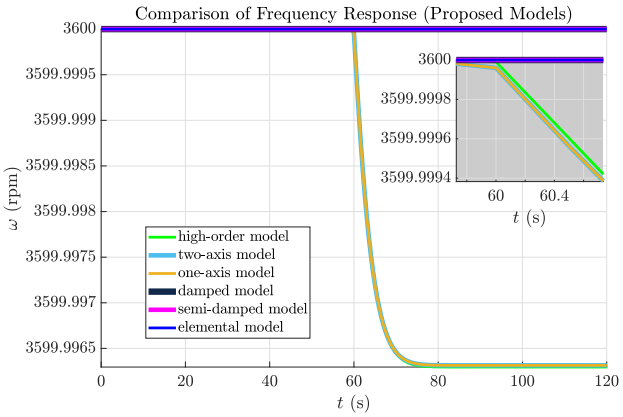

(b) The proposed models.

Fig. 11: Second Test Scenario: Angular frequency response of the classical model and the proposed models in comparison with those of the two-axis model, the one-axis model, and the high-order model.

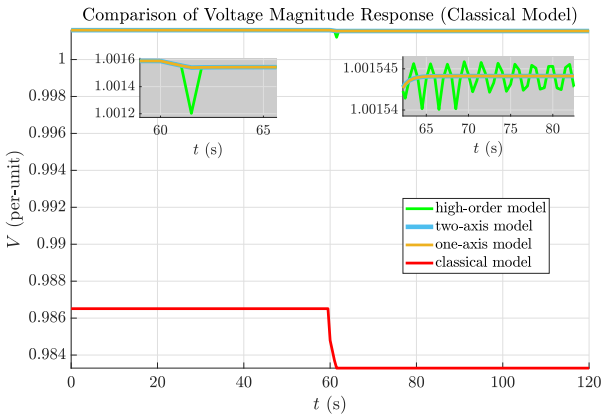

(a) The classical models.

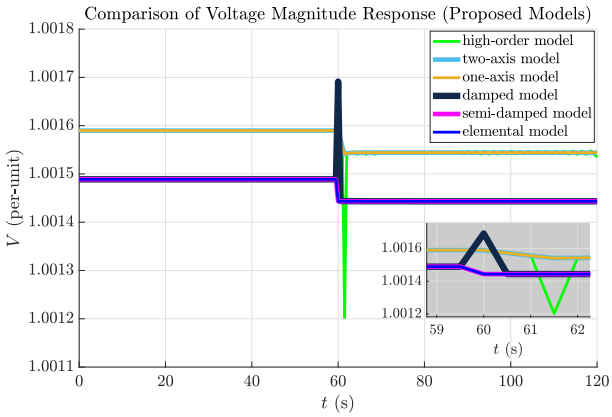

(b) The proposed model.

Fig. 12: Second Test Scenario: Voltage magnitude response of the classical model and the proposed models in comparison with those of the two-axis model, the one-axis model, and the high-order model.

where

$$E_{d'}^{(0)}(t) = \frac{X_q - X_{q'}}{X_q} V_d - \frac{X_k(X_q - X_{q'})N_q}{D_q}\dot{V}_d,$$
$$E_{d'}^{(1)}(t) = -\frac{M_q}{X_q D_q}\dot{V}_d + \boldsymbol{\mathcal{O}}\left(\tau_{q'}\right),$$

so that

$$E_{d'} \approx \frac{X_q - X_{q'}}{X_q} V_d - \left(\frac{X_k(X_q - X_{q'})N_q}{D_q} + \frac{\tau_{q'} M_q}{X_q D_q}\right)\dot{V}_d, \tag{23}$$

where

$$N_q \coloneqq \tau_{q'}\tau_{q''} X_{q'}(X_{q'} - X_{q''})(X_{q'} - X_k),$$
$$D_q \coloneqq \tau_{q'} X_q (X_{q'})^2 (X_{q'} - X_k)^2 - \tau_{q''} X_q (X_k)^2 (X_q - X_{q'})(X_{q'} - X_{q''}),$$
$$M_q \coloneqq \tau_{q'} (X_{q'})^3 (X_q - X_{q'})(X_{q'} - X_k)^2.$$

Finally, for the other fast states, i.e., $E_{q'}$, E_f, U_f, $\bar{U}_f$, T_m, P_u, P_{a_1}, P_{a_2}, P_{b_1}, and P_{b_2}, we derive the following zero-order approximations of their manifolds by employing singular perturbation analysis, as described in Section IV-B, on (4), (9), and (11):

$$\begin{aligned}
E_{q'} &\approx E_{q'}^{(0)}(t) = \frac{X_{d'} K_u}{X_d K_f}(E_r - E) + \frac{X_d - X_{d'}}{X_d} V_q \\
&\quad - \frac{X_k(X_d - X_{d'})N_d}{D_d}\dot{V}_q, \\
E_f &\approx E_f^{(0)}(t) = \frac{K_u}{K_f}(E_r - E), \\
U_f &\approx U_f^{(0)}(t) = K_u(E_r - E), \\
\bar{U}_f &\approx \bar{U}_f^{(0)}(t) = \frac{\bar{K}_u K_u}{\bar{\tau}_u K_f}(E_r - E), \\
T_m &\approx T_m^{(0)}(t) = P_c - \bar{D}_0(\omega - \omega_0), \\
P_u &\approx P_u^{(0)}(t) = P_c - \bar{D}_0(\omega - \omega_0), \\
P_{a_1} &\approx P_{a_1}^{(0)}(t) = 0, \qquad P_{a_2} \approx P_{a_2}^{(0)}(t) = 0, \\
P_{b_1} &\approx P_{b_1}^{(0)}(t) = 0, \qquad P_{b_2} \approx P_{b_2}^{(0)}(t) = 0,
\end{aligned} \tag{24}$$

where

$$N_d \coloneqq \tau_{d'}\tau_{d''} X_{d'}(X_{d'} - X_{d''})(X_{d'} - X_k),$$

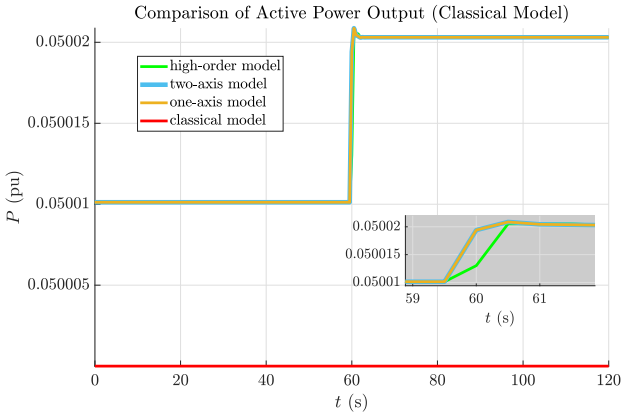

(a) The classical models.

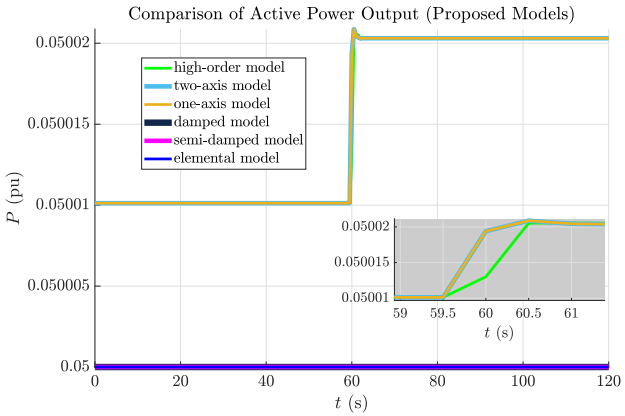

(b) The proposed model.

Fig. 13: Second Test Scenario: Active power output response of the classical model and the proposed models in comparison with those of the two-axis model, the one-axis model, and the high-order model.

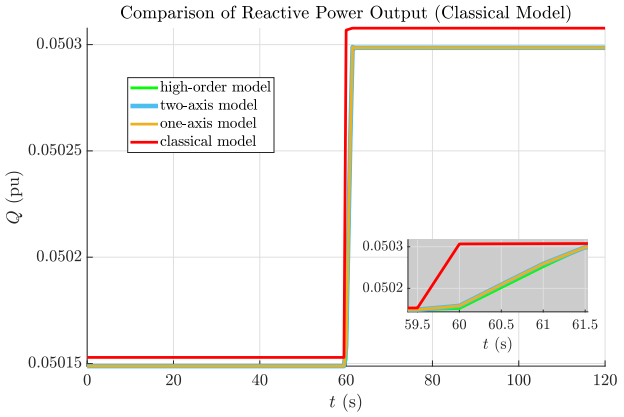

(a) The classical models.

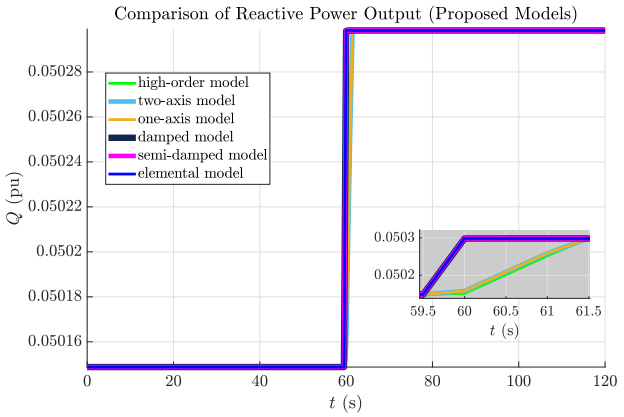

(b) The proposed model.

Fig. 14: Second Test Scenario: Reactive power output response of the classical model and the proposed models in comparison with those of the two-axis model, the one-axis model, and the high-order model.

$$D_d \coloneqq \tau_{d'} X_d (X_{d'})^2 (X_{d'} - X_k)^2 - \tau_{d''} X_d (X_k)^2 (X_d - X_{d'})(X_{d'} - X_{d''}).$$

D. The Elemental Model

To formulate the elemental model from the high-order model, the differential equations for the slow states, i.e., (2) and (10), are retained, but the differential equations for all fast states are replaced with zero-order approximations of their manifolds. These approximations are obtained from the expressions in (21), (22), (23), and (24) by setting $\tau_{q''} = 0$, $\tau_{d''} = 0$, and $\tau_{q'} = 0$ to give:

$$\Psi_q \approx -V_d, \qquad \Psi_d \approx V_q, \qquad \Phi_q \approx E_d - V_d, \tag{25}$$

$$\Phi_{q_2} \approx -\frac{X_q - X_k}{X_q} V_d, \tag{26}$$

$$\Phi_{d_1} \approx \frac{X_d - X_k}{X_d} V_q + \frac{X_k K_u}{X_d K_f}(E_r - E), \tag{27}$$

$$E_{d'} \approx \frac{X_q - X_{q'}}{X_q} V_d, \tag{28}$$

$$E_{q'} \approx \frac{X_d - X_{d'}}{X_d} V_q + \frac{X_{d'} K_u}{X_d K_f}(E_r - E), \tag{29}$$

$$E_f \approx \frac{K_u}{K_f}(E_r - E), \qquad U_f \approx K_u(E_r - E), \tag{30}$$

$$\bar{U}_f \approx \frac{\bar{K}_u K_u}{\bar{\tau}_u K_f}(E_r - E), \quad T_m \approx P_c - \bar{D}_0(\omega - \omega_0), \tag{31}$$

$$P_u \approx P_c - \bar{D}_0(\omega - \omega_0), \quad P_{a_1} \approx 0, \quad P_{a_2} \approx 0, \tag{32}$$

$$P_{b_1} \approx 0, \qquad P_{b_2} \approx 0, \qquad \Phi_d \approx -E_q + V_q. \tag{33}$$

Using these approximations, from (5), it follows that

$$I_q = \frac{1}{X_q} V_d, \tag{34}$$

$$I_d = -\frac{1}{X_d} V_q + \frac{K_u}{K_f X_d}(E_r - E). \tag{35}$$

Combining these manifold approximation expressions for the fast states with the differential equations that describe the slow state dynamics, i.e., (2) and (10), the elemental model of a

synchronous machine is given by:

$$\begin{aligned}\dot{\delta} &= \omega - \omega_0,\\ M\dot{\omega} &= P_c - \bar{D}_0(\omega-\omega_0) - \frac{X_d - X_q}{2X_qX_d}V^2\sin 2(\delta-\theta)\\ &\quad - \frac{K_u}{K_fX_d}(E_r - E)V\sin(\delta-\theta) - \tilde{D}_0\omega.\end{aligned} \tag{36}$$

E. The Semi-Damped Model

To formulate the semi-damped model from the high-order model, the differential equations for the slow states, i.e., (2) and (10), are retained, but the differential equations for all fast states, except $E_{d'}(t)$, i.e., the slower damper winding state, are replaced with zero-order approximations of their manifolds. The differential equation (4), which describes the dynamics of $E_{d'}(t)$, is replaced with a first-order approximation of the manifold for $E_{d'}(t)$. These approximations are obtained from the expressions in (21), (22), (23), and (24) by setting $\tau_{q''} = 0$ and $\tau_{d''} = 0$ to give:

$$\Psi_q \approx -V_d, \qquad \Psi_d \approx V_q, \qquad \Phi_q \approx E_d - V_d, \tag{37}$$

$$\Phi_{q_2} \approx -\frac{X_q - X_k}{X_q}V_d + \frac{\tau_{q'}X_k(X_q - X_{q'})}{X_q^2}\dot{V}_d, \tag{38}$$

$$\Phi_{d_1} \approx \frac{X_d - X_k}{X_d}V_q + \frac{X_kK_u}{X_dK_f}(E_r - E), \tag{39}$$

$$E_{d'} \approx \frac{X_q - X_{q'}}{X_q}V_d - \tau_{q'}\frac{X_{q'}(X_q - X_{q'})}{X_q^2}\dot{V}_d, \tag{40}$$

$$E_{q'} \approx \frac{X_d - X_{d'}}{X_d}V_q + \frac{X_{d'}K_u}{X_dK_f}(E_r - E), \tag{41}$$

$$E_f \approx \frac{K_u}{K_f}(E_r - E), \qquad U_f \approx K_u(E_r - E), \tag{42}$$

$$\bar{U}_f \approx \frac{\bar{K}_uK_u}{\bar{\tau}_uK_f}(E_r - E), \quad T_m \approx P_c - \bar{D}_0(\omega - \omega_0), \tag{43}$$

$$P_u \approx P_c - \bar{D}_0(\omega-\omega_0), \quad P_{a_1} \approx 0, \quad P_{a_2} \approx 0, \tag{44}$$

$$P_{b_1} \approx 0, \qquad P_{b_2} \approx 0, \qquad \Phi_d \approx -E_q + V_q. \tag{45}$$

Using these approximations, from (5), it follows that

$$I_q = \frac{1}{X_q}V_d + \frac{\tau_{q'}(X_q - X_{q'})}{X_q^2}\dot{V}_d, \tag{46}$$

$$I_d = -\frac{1}{X_d}V_q + \frac{K_u}{K_fX_d}(E_r - E). \tag{47}$$

Combining these manifold approximation expressions for the fast states with the differential equations that describe the slow state dynamics, i.e., (2) and (10), the semi-damped model of a synchronous machine is given by:

$$\begin{aligned}\dot{\delta} &= \omega - \omega_0,\\ M\dot{\omega} &= P_c - \bar{D}_0(\omega-\omega_0) - \frac{X_d - X_q}{2X_qX_d}V^2\sin 2(\delta-\theta)\\ &\quad - \frac{K_u}{K_fX_d}(E_r - E)V\sin(\delta-\theta) - \tilde{D}_0\omega\\ &\quad - \frac{\tau_{q'}(X_q - X_{q'})}{2X_q^2}\dot{V}V\sin 2(\delta-\theta)\\ &\quad - \frac{\tau_{q'}(X_q - X_{q'})}{X_q^2}V^2\cos^2(\delta-\theta)(\dot{\delta}-\dot{\theta}).\end{aligned} \tag{48}$$

F. The Damped Model

To formulate the damped model from the high-order model, the differential equations for the slow states, i.e., (2) and (10), are retained, but the differential equations for all fast states, except the damper windings states, are replaced with zero-order approximations of their manifolds. Equations (7) and (8), which describe the damper winding dynamics, are replaced with first-order approximations of the manifolds for $\Phi_{q_2}(t)$, $\Phi_{d_1}(t)$, and $E_{d'}(t)$. The following expressions for these manifold approximations can be obtained from (21), (22), (23), and (24):

$$\Psi_q \approx -V_d, \qquad \Psi_d \approx V_q, \qquad \Phi_q \approx E_d - V_d, \tag{49}$$

$$\Phi_{q_2} \approx -\frac{X_q - X_k}{X_q}V_d + \frac{\tau_{q''}X_{q''}(X_{q'} - X_k)}{(X_{q'})^2}\dot{V}_d \tag{50}$$

$$+ \frac{(X_q - X_{q'})(\tau_{q'}X_{q'}^2X_k^2 + \tau_{q''}X_{q''}X_k^2X_q)N_q}{\tau_{q'}X_{q'}^3D_q}\dot{V}_d \tag{51}$$

$$+ \frac{(\tau_{q'}(X_{q'})^2X_k + \tau_{q''}X_{q''}X_kX_q)M_q}{X_{q'}^3X_qD_q}\dot{V}_d, \tag{52}$$

$$\Phi_{d_1} \approx \frac{X_d - X_k}{X_d}V_q - \frac{\tau_{d''}X_{d''}(X_{d'} - X_k)}{X_{d'})^2}\dot{V}_q \tag{53}$$

$$- \frac{(X_d - X_{d'})(\tau_{d'}X_{d'}^2X_k^2 + \tau_{d''}X_{d''}X_k^2X_d)N_d}{\tau_{d'}X_{d'}^3D_d}\dot{V}_q \tag{54}$$

$$+ \frac{X_kK_u}{X_dK_f}(E_r - E), \tag{55}$$

$$E_{d'} \approx \frac{X_q - X_{q'}}{X_q}V_d - \left(\frac{X_k(X_q - X_{q'})N_q}{D_q} + \frac{\tau_{q'}M_q}{X_qD_q}\right)\dot{V}_d, \tag{56}$$

$$E_{q'} \approx \frac{X_d - X_{d'}}{X_d}V_q - \frac{N_d}{D_d}\dot{V}_q + \frac{X_{d'}K_u}{X_dK_f}(E_r - E), \tag{57}$$

$$E_f \approx \frac{K_u}{K_f}(E_r - E), \qquad U_f \approx K_u(E_r - E), \tag{58}$$

$$\bar{U}_f \approx \frac{\bar{K}_uK_u}{\bar{\tau}_uK_f}(E_r - E), \quad T_m \approx P_c - \bar{D}_0(\omega - \omega_0), \tag{59}$$

$$P_u \approx P_c - \bar{D}_0(\omega-\omega_0), \quad P_{a_1} \approx 0, \quad P_{a_2} \approx 0, \tag{60}$$

$$P_{b_1} \approx 0, \qquad P_{b_2} \approx 0, \qquad \Phi_d \approx -E_q + V_q. \tag{61}$$

Using these approximations, from (5), it follows that

$$I_q = \frac{1}{X_q}V_d + \frac{\tau_{q'}M_q}{X_qX_{q'}D_q}\dot{V}_d + \frac{X_k(X_q - X_{q'})N_q}{X_{q'}D_q}\dot{V}_d \tag{62}$$

$$+ \frac{(X_q - X_k)N_q}{D_q}\dot{V}_d, \tag{63}$$

$$I_d = -\frac{1}{X_d}V_q + \frac{K_u}{K_fX_d}(E_r - E) - \frac{(X_d - X_k)N_d}{D_d}\dot{V}_q. \tag{64}$$

Combining these manifold approximation expressions for the fast states with the differential equations that describe the slow state dynamics, i.e., (2) and (10), the damped model of a

synchronous machine is given by:

$$\begin{aligned}
\dot{\delta} &= \omega - \omega_0, \\
M\dot{\omega} &= P_c - \bar{D}_0(\omega - \omega_0) - \frac{X_d - X_q}{2X_qX_d}V^2 \sin 2(\delta - \theta) \\
&\quad - \frac{K_u}{K_fX_d}(E_r - E)V \sin(\delta - \theta) - \tilde{D}_0\omega \\
&\quad - \frac{K_q - K_d}{2}\dot{V}V \sin 2(\delta - \theta) \\
&\quad - K_qV^2 \cos^2(\delta - \theta)(\dot{\delta} - \dot{\theta}) \\
&\quad - K_dV^2 \sin^2(\delta - \theta)(\dot{\delta} - \dot{\theta}).
\end{aligned} \tag{65}$$

where

$$K_q \coloneqq \frac{\tau_{q'}M_q + X_qX_k(X_q - X_{q'})N_q + X_qX_{q'}(X_q - X_k)N_q}{X_qX_{q'}D_q},$$
$$K_d \coloneqq \frac{(X_d - X_k)N_d}{D_d}.$$

V. Concluding Remarks

In this paper, we introduced three second-order synchronous machine models referred to as the elemental model, the damped model, and the semi-damped model. We showed how these models, and the so-called classical model, can be derived from a high-order machine model. While the classical model is obtained by identifying small and large parameters in the high-order model, and setting them to zero and infinity, respectively, the library of second-order models are obtained by identifying fast and slow states in the high-order model, and replacing differential equations for the fast states with algebraic counterparts, referred to as manifold approximations (zero-order or first-order). Also, the voltage magnitude, angular frequency, and phase response of our proposed models were shown to closely match that of the high-order model from which they were derived, as well as that of other previously developed reduced order models.

For a generator that is connected to an electrical network bus, if the derivative of the bus voltage magnitude is known, then the semi-damped model would provide improved simulation accuracy, compared to the elemental model, and the damped model would provide the best accuracy. Although it is hard to confirm this statement experimentally or through simulations, because the derivative of the bus voltage magnitude is difficult to compute, it can be verified mathematically using the formulations in Section IV, or by using the results presented in Table I. In Table I, it can be observed that the elemental model is derived from the semi-damped model by setting the $\mathcal{O}(\epsilon)$ term $\tau_{q'}$ to zero, and the semi-damped model can be derived from the damped model by setting $\mathcal{O}(\epsilon)$ terms $\tau_{q''}$ and $\tau_{d''}$ to zero. Each approximation of these $\mathcal{O}(\epsilon)$ terms introduces an $\mathcal{O}(\epsilon)$ error in the resulting model.

Generally speaking, the proposed second-order models are applicable for power system analysis and control design tasks with time-scales greater than five seconds. Some examples of such tasks include, but are not limited to, electromechanical transient stability studies, frequency control design, and voltage stability studies.

References

[1] P. Kundur, N. J. Balu, and M. G. Lauby, *Power system stability and control*. McGraw-Hill, 1994.

[2] P. Sauer and A. Pai, *Power System Dynamics and Stability*. Stipes Publishing L.L.C., 2006.

[3] P. Krause, O. Wasynczuk, S. Sudhoff, and S. Pekarek, *Analysis of Electric Machinery and Drive Systems*, ser. IEEE Press Series on Power Engineering. Wiley, 2013.

[4] L. Wang, J. Jatskevich, and H. W. Dommel, "Re-examination of synchronous machine modeling techniques for electromagnetic transient simulations," *IEEE Transactions on Power Systems*, vol. 22, no. 3, pp. 1221–1230, Aug. 2007.

[5] S. Crary, *Power System Stability: Transient stability*, ser. General Electric series. John Wiley, 1947.

[6] E. Kimbark, *Power Systems Stability. Vol. 3. Synchronous Machines*. Wiley, 1956.

[7] A. R. Bergen and D. J. Hill, "A structure preserving model for power system stability analysis," *IEEE Transactions on Power Apparatus and Systems*, vol. PAS-100, no. 1, pp. 25–35, Jan 1981.

[8] Z. Qu, J. F. Dorsey, J. Bond, and J. D. McCalley, "Application of robust control to sustained oscillations in power systems," *IEEE Transactions on Circuits and Systems I: Fundamental Theory and Applications*, vol. 39, no. 6, pp. 470–476, June 1992.

[9] A. Bergen and V. Vittal, *Power Systems Analysis*. Prentice Hall, 2000.

[10] D. Subbarao and K. K. Singh, "Hysteresis and bifurcations in the classical model of generator," *IEEE Transactions on Power Systems*, vol. 19, no. 4, pp. 1918–1924, Nov 2004.

[11] C. Qi, K. Wang, and G. Li, "Parameter space and rotor angle stability control of virtual synchronous machine," in *2018 IEEE Power Energy Society General Meeting (PESGM)*, Aug 2018, pp. 1–5.

[12] A. Pai, *Energy Function Analysis for Power System Stability*, ser. Power Electronics and Power Systems. Springer, Boston, MA, 1989.

[13] P. M. Anderson and A. A. Fouad, *Power system control and stability*, ser. IEEE Press power engineering series. IEEE Press, 2003.

[14] S. Y. Caliskan and P. Tabuada, "Uses and abuses of the swing equation model," in *Proc. of IEEE Conference on Decision and Control (CDC)*, Dec 2015, pp. 6662–6667.

[15] O. Ajala, A. D. Domínguez-García, P. W. Sauer, and D. Liberzon, "A second-order synchronous machine model for multi-swing stability analysis," in *Proc. of the North American Power Symposium, Wichita, KS*, Dec. 2018, pp. 1586–1591.

[16] T. Weckesser, H. Jóhannsson, and J. Østergaard, "Impact of model detail of synchronous machines on real-time transient stability assessment," in *Proc. of the IREP Symposium Bulk Power System Dynamics and Control - IX Optimization, Security and Control of the Emerging Power Grid*, Aug 2013, pp. 1–9.

[17] P. Kokotović, H. K. Khalil, and J. O'Reilly, *Singular Perturbation Methods in Control: Analysis and Design*, ser. Classics in Applied Mathematics. Society for Industrial and Applied Mathematics, 1986.

[18] H. Khalil, *Nonlinear Systems*, 3rd ed. Prentice Hall, 2002.

[19] J. H. Chow, *Time-Scale Modeling of Dynamic Networks with Applications to Power Systems*, B. A.V. and T. M., Eds. Springer, 1982.

[20] P. W. Sauer, S. Ahmed-Zaid, and P. V. Kokotovic, "An integral manifold approach to reduced order dynamic modeling of synchronous machines," *IEEE Transactions on Power Systems*, vol. 3, no. 1, pp. 17–23, Feb. 1988.

[21] P. V. Kokotovic and P. W. Sauer, "Integral manifold as a tool for reduced-order modeling of nonlinear systems: A synchronous machine case study," *IEEE Transactions on Circuits and Systems*, vol. 36, no. 3, pp. 403–410, Mar. 1989.

[22] O. Ajala, A. D. Domínguez-García, P. W. Sauer, and D. Liberzon, "A second-order synchronous machine model for multi-swing stability analysis," in *Proc. of the North American Power Symposium (NAPS)*, Dec. 2019, pp. 1586–1591.

[23] "IEEE Recommended Practice for Excitation System Models for Power System Stability Studies," *IEEE Std 421.5-2016 (Revision of IEEE Std 421.5-2005)*, pp. 1–207, Aug. 2016.

[24] PowerWorld corporation. (2017) Woodward diesel governor model. [Online]. Available: {https://www.powerworld.com}

[25] A. Fouad and V. Vittal, *Power System Transient Stability Analysis Using the Transient Energy Function Method*. Prentice Hall, 1992.